Water vapor at the tropopause during the CRISTA 2 mission

D. Offermann,[1] B. Schaeler,[1] M. Riese,[2] M. Langfermann,[3] M. Jarisch,[1] G. Eidmann,[4] C. Schiller,[2] H. G. J. Smit,[2] and W. G. Read[5]

Received 29 March 2001; revised 29 August 2001; accepted 30 August 2001; published 18 September 2002.

[1] Water vapor mixing ratios at the tropopause are derived as a new Cryogenic Infrared Spectrometers and Telescopes for the Atmosphere (CRISTA) data product from limb scan measurements of the second mission. Global maps are obtained on a daily basis. Data loss due to high clouds is found to be moderate. Good agreement with in situ airplane measurements (Fast In Situ Stratospheric Hygrometer (FISH)) is obtained for these Version 1 data. A number of different analyses are performed to show the research potential of the data product: the CRISTA data are compared to measurements of the Microwave Limb Sounder (MLS) instrument on the Upper Atmosphere Research Satellite (UARS). Version 4.9 climatology data and Version 5 coincident measurements are used. Good agreement of CRISTA and Version 4.9 data is obtained, whereas there are differences with respect to the Version 5.0 data. CRISTA finds vapor mixing ratios to be highly variable. Only a small part of this is instrumental. Variability is structured, and a scaling behavior is observed. Relation to convectively generated gravity waves is discussed. Relative humidity (RH) is determined on the basis of the CRISTA data. Suitability for supersaturation statistics is discussed and appears to be limited. CRISTA water vapor data are assimilated into a 3D transport model driven by UK Meteorological Office (UKMO) winds. Results are discussed in terms of meridional transports and atmospheric diffusivities. Diffusivities appear to be connected with the water vapor variances in a simple manner. *INDEX TERMS:* 0341 Atmospheric Composition and Structure: Middle atmosphere—constituent transport and chemistry (3334); 0368 Atmospheric Composition and Structure: Troposphere—constituent transport and chemistry; 3362 Meteorology and Atmospheric Dynamics: Stratosphere/troposphere interactions; *KEYWORDS:* water vapor, tropopause, CRISTA, trace gas variability, constituent transport, middle atmosphere dynamics

Citation: Offermann, D., B. Schaeler, M. Riese, M. Langfermann, M. Jarisch, G. Eidmann, C. Schiller, H. G. J. Smit, and W. G. Read, Water vapor at the tropopause during the CRISTA 2 mission, *J. Geophys. Res.*, *107*(D23), 8176, doi:10.1029/2001JD000700, 2002.

1. Introduction

[2] Water vapor in the upper troposphere and lower stratosphere plays a very important role in the energy budget, dynamics, and chemistry of the atmosphere. This role is, however, not well understood in several respects. For climate prediction, for instance, it is important to know whether water vapor provides a positive or a negative feedback with increasing temperatures. This is an open question as yet, and a high measurement accuracy is required to contribute to this problem. (For details and a recent literature survey, see *Kley et al.* [2000].) Detailed questions in the tropopause region concern the nature of the hygropause [e.g., *Teitelbaum et al.*, 2000], the outgoing longwave radiation (OLR) in dependence of upper troposphere humidity changes [e.g., *McCormack et al.*, 2000], and the occurrence of humidity supersaturation [e.g., *Jensen et al.*, 1999; *Rosenfeld and Woodley*, 2000; *Gierens et al.*, 1999, 2000].

[3] The nature of the tropopause itself is not completely understood [e.g., *Mahlman*, 1997]. There are a number of different definitions of the tropopause, which use the temperature, the vertical temperature gradient, the potential vorticity, or—most recently—the atmospheric diffusivity [*Haynes and Shuckburgh*, 2000]. The latter analysis suggests to defining the tropopause as a transport barrier (minimum of eddy diffusivity K_{eff}). This is a partial aspect of the larger question how air is transported and exchanged between the troposphere and the stratosphere (overworld and lowermost stratosphere) on large, medium, and small scales [e.g., *Holton et al.*, 1995; *Chen*, 1995]. Water vapor is a valuable tracer for such dynamical analyses [e.g., *Pan et al.*, 1997, 2000; *Ovarlez et al.*, 1999; *Dessler and Kim*, 1999; *McCormack et al.*, 2000; *Udelhofen and Hartmann*, 1995] (for a recent review of the extensive literature, see *Kley et al.* [2000]). Water vapor also plays an important role in atmospheric chemistry, as it is a precursor of hydroxyl [e.g., *Spivakovsky et al.*, 2000].

[1]Department of Physics, University of Wuppertal, Wuppertal, Germany.
[2]Institute of Chemistry and Dynamics of the Geosphere, Research Center Juelich GmbH, Juelich, Germany.
[3]Daimler-Benz-Aerospace, Dornier GmbH, Friedrichshafen, Germany.
[4]Vacuumschmelze & CoKG, Hanau, Germany.
[5]Jet Propulsion Laboratory, Pasadena, California, USA.

0148-0227/02/2001JD000700$09.00

[4] To be useful near the tropopause water vapor measurements need to have high accuracy (3–10%) [*Kley et al.*, 2000]. This is difficult to achieve because (1) water vapor is not easily measured, (2) the water vapor gradient is very steep near the tropopause, and (3) water vapor variability is very high at these altitudes. In addition satellite measurements can be hampered by high clouds. In consequence the data set of reliable measurements in the upper troposphere and in the lowest stratosphere is not large.

[5] Global water vapor mixing ratios near the tropopause were and are measured by satellite instruments such as the Microwave Limb Sounder (MLS) [e.g., *Stone et al.*, 2000] and the Halogen Occultation Experiment (HALOE) [*Remsberg et al.*, 1996; *Dessler and Kim*, 1999] on the Upper Atmosphere Research Satellite (UARS), and by the Stratospheric Aerosol and Gas Experiment II (SAGE II) [*Chiou et al.*, 1997] on the Earth Radiation Budget Satellite (ERBS). More recently the Polar Ozone and Aerosol Measurement (POAM III) also provided low-altitude water vapor data [e.g., *Nedoluha et al.*, 2000]. Water vapor data were also obtained from the Atmospheric Trace Molecule Spectroscopy (ATMOS) experiment flown on the ATLAS-3 Space Shuttle mission STS 66 [*Abbas et al.*, 1996]. In situ measurements are taken by radiosondes, airplanes, and balloons. Various types of instruments are used such as the frost point hygrometer [e.g., *Ovarlez et al.*, 2000], tunable diode laser [e.g., *Vay et al.*, 2000], differential absorption lidar (DIAL) [*Ehret et al.*, 1999], Lyman-α instruments [e.g., *Hintsa et al.*, 1999; *Zoeger et al.*, 1999], and the MOZAIC instrument set (Measurement of Ozone by Airbus In-Service Aircraft) [*Helten et al.*, 1998, 1999]. A comprehensive survey of water vapor measurements was recently given by *Kley et al.* [2000].

[6] The present paper presents water vapor mixing ratios at the tropopause as obtained during the second mission of the Cryogenic Infrared Spectrometers and Telescopes for the Atmosphere (CRISTA) (7–19 August 1997). CRISTA is a limb-scanning instrument with three infrared telescopes for increased spatial resolution and high data density. The optics include four IR spectrometers and are helium cooled, which yields high measurement speed and good signal-to-noise ratio. The instrument is taken to a 300 km altitude, 57° inclination orbit by the Space Shuttle. It is released from the Shuttle cargo bay for an autonomous flight of several days, during which it can be oriented to any direction desired. A fairly large latitude coverage of ±74° is obtained this way. At the end of the mission CRISTA is retrieved by the Shuttle and brought back to Earth for recalibration. Details of the instrument and the mission are given by *Offermann et al.* [1999] and by *Grossmann et al.* [2002], respectively.

[7] The paper is organized as follows: In the second section the measurements are described and results are compared to simultaneous in situ measurements. Examples are given of the water vapor distribution and its structural appearance. In the third section several examples of analyses are given for which the CRISTA data may be suitable. Mostly, CRISTA data on the 215 hPa (11–12 km) level are used, i.e., somewhat above or below the tropopause, depending on latitude. The first example is the intercomparison with simultaneous satellite data at small miss-distances and miss-times that were taken by the MLS instrument on UARS. Second, the water vapor variability is analyzed to some extent using a structure function. Thirdly, the suitability of the CRISTA limb scan data for humidity supersaturation statistics is discussed. Fourthly, the data are assimilated into a 3D transport model, and suitability of the results for transport analyses is discussed. Last, fluctuations of the CRISTA data are compared to eddy diffusivities recently published. In the fourth section a few conclusions are drawn.

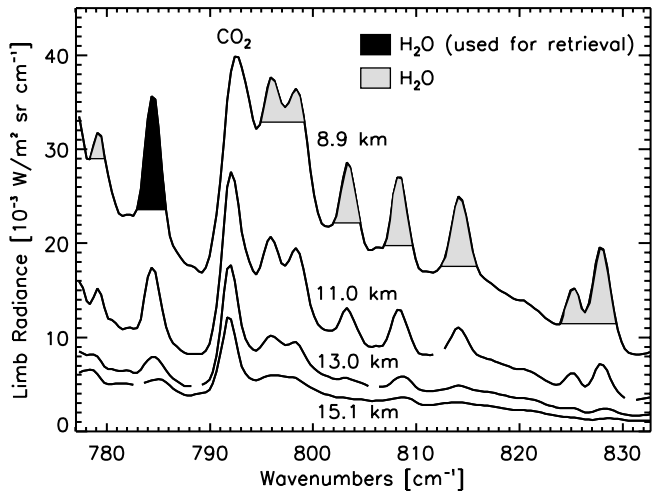

Figure 1. Emission spectra at low altitudes showing water vapor lines. Line at 784 cm^{-1} is used for H_2O retrieval.

[8] The basic intention of the paper is to introduce tropopause water vapor as a new CRISTA data product specific for the second mission, and indicate a number of applications. This is in line with the other papers of this special issue, which present an overview of the second CRISTA mission [*Grossmann et al.*, 2002]. The data presented here can be obtained from our ftp site. See www.crista.uni-wuppertal.de for details.

2. Measurements and Results

[9] During the first CRISTA mission the measurements covered an altitude range from 16 to 160 km approximately [*Riese et al.*, 1999a]. During the second mission this range was extended downward to 11 km routinely, and reached as low as 7 km in a special measurement mode [*Grossmann et al.*, 2002]. This allowed water vapor measurements well below the tropopause in a large part of the global atmosphere. Water vapor mixing ratios were derived from 6.3 μm wavelength emissions at 20 km altitude and above. At lower heights these emissions become optically thick, and a water line at 12.7 μm had to be used instead. Figure 1 shows respective low-altitude spectra at four different heights measured during one altitude scan. Water vapor emission features are indicated by light shading. The line used for H_2O retrieval is marked by heavy shading.

[10] The picture shows that intensities are high at these altitudes and hence the spectra have a very reasonable signal-to-noise ratio (about 300). The geometric field of view (FOV) of the three CRISTA telescopes is $\leq$1.5 km in the vertical, and the altitude steps during a vertical scan are about 2 km. Vertical mixing ratio profiles are obtained from these radiances by an onion-peeling technique. A multiple-

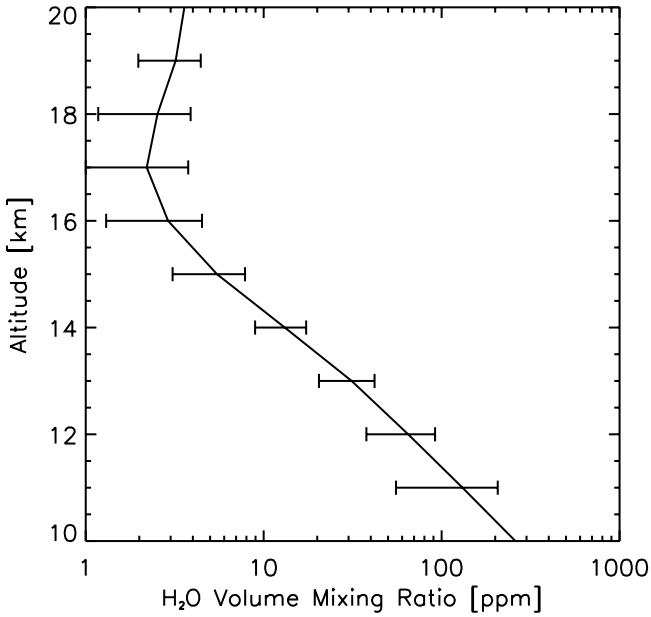

Figure 2. Water vapor volume mixing ratio versus altitude. A zonal mean for 10°S–30°N on 11/12 August 1997 (24 hours of measurement) is given. Bars show the data scatter, which is mostly from atmospheric variability.

emitter, multiple-spectral-sampling-point algorithm is used. Details of this retrieval were described by *Schaeler and Riese* [2001]. A corresponding altitude profile is shown in Figure 2. A zonal mean profile (10°S–30°N) is given, which results from more than 450 single profiles.

[11] The limb scan technique by its nature integrates the signal from the atmosphere over some distance along the view direction in the vicinity of the tangent point. This integration length is dependent on the vertical gradient of the mixing ratio of the constituent to be measured. For a gas with a gradient as steep as that shown in Figure 2 this length is about 150 km. The horizontal extension of the field of view across the view direction is about 20 km. Hence the footprint of the water vapor measurement is about 150 × 20 km. Due to the steepness of the water profile the geometric FOV of CRISTA is not illuminated homogeneously. Most of the radiation is in the lower third of the FOV, and hence the effective vertical resolution of the measurement is smaller than 1.5 km. It is estimated to be less than 0.5 km. The spatial atmospheric volume sensed by one CRISTA spectrum thus has the effective dimensions 150 × 20 × 0.5 km.

[12] The bars in Figure 2 represent the variability of the data (standard deviation), which includes atmospheric as well as instrumental scatter. The instrument precision is mainly determined by the precision of view direction during the limb scan, i.e., by the altitude noise of the tangent height at which the measurement is taken. This noise is 60 m only. (Absolute altitude accuracy is about 100 m.) Nevertheless it translates into a relatively large measurement uncertainty because of the great steepness of the water vapor profile. The CRISTA data are still somewhat preliminary (Version 1 data). The CRISTA precision is estimated to be 11% at this stage. This figure includes spectral inaccuracies and detector noise. Comparison with the scatter bars in Figure 2 shows that by far the largest part of the variability seen must be of atmospheric origin.

[13] The absolute accuracy of the CRISTA data at this stage is estimated to be 22%. Improved accuracy is expected for a future data version. For validation purposes the CRISTA water vapor measurements near the tropopause were compared with in situ measurements taken by a fluorescence technique. The Fast In Situ Stratospheric

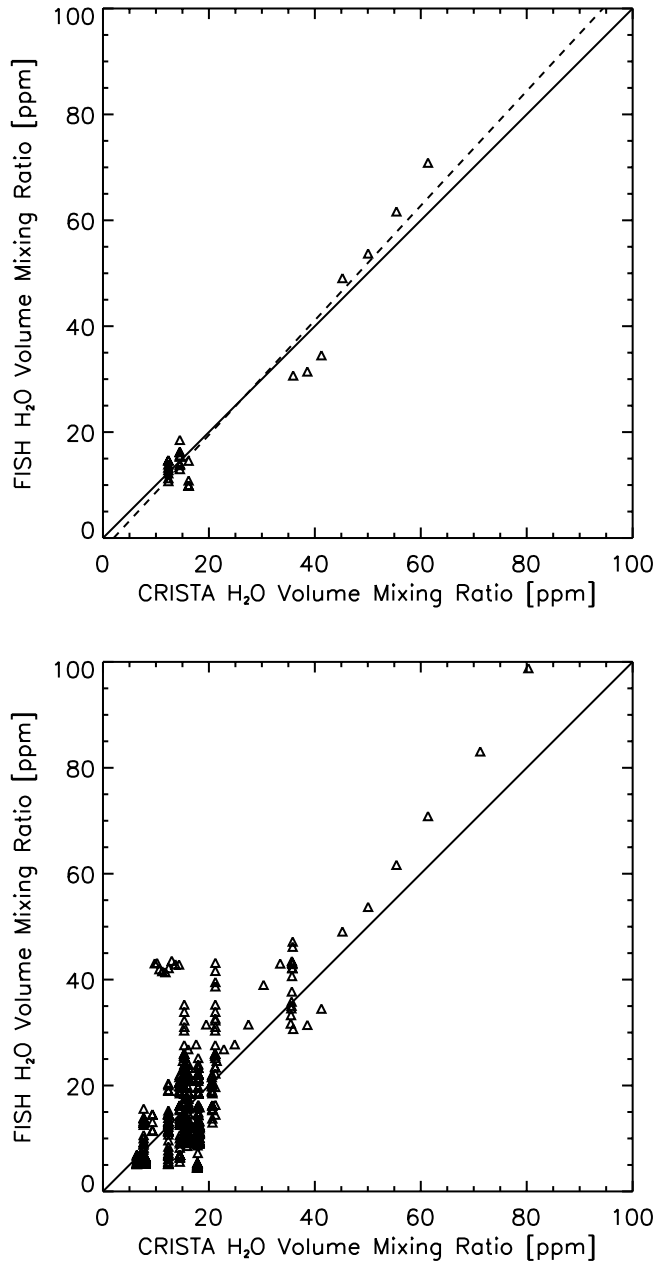

Figure 3. (a, top) Coincidences of CRISTA and FISH airplane measurements. Volume mixing ratios are given in ppm. Miss-distance is less than 50 km and miss-time less than 2 hours. Altitude range is 175–225 hPa. Correlation coefficient is 0.97. In total, 28 coincidences are shown (see text). (b, bottom) As in (a), but with miss-distance less than 200 km. Altitude range is 160–280 hPa. Correlation coefficient is 0.93 and the number of coincidences is 413.

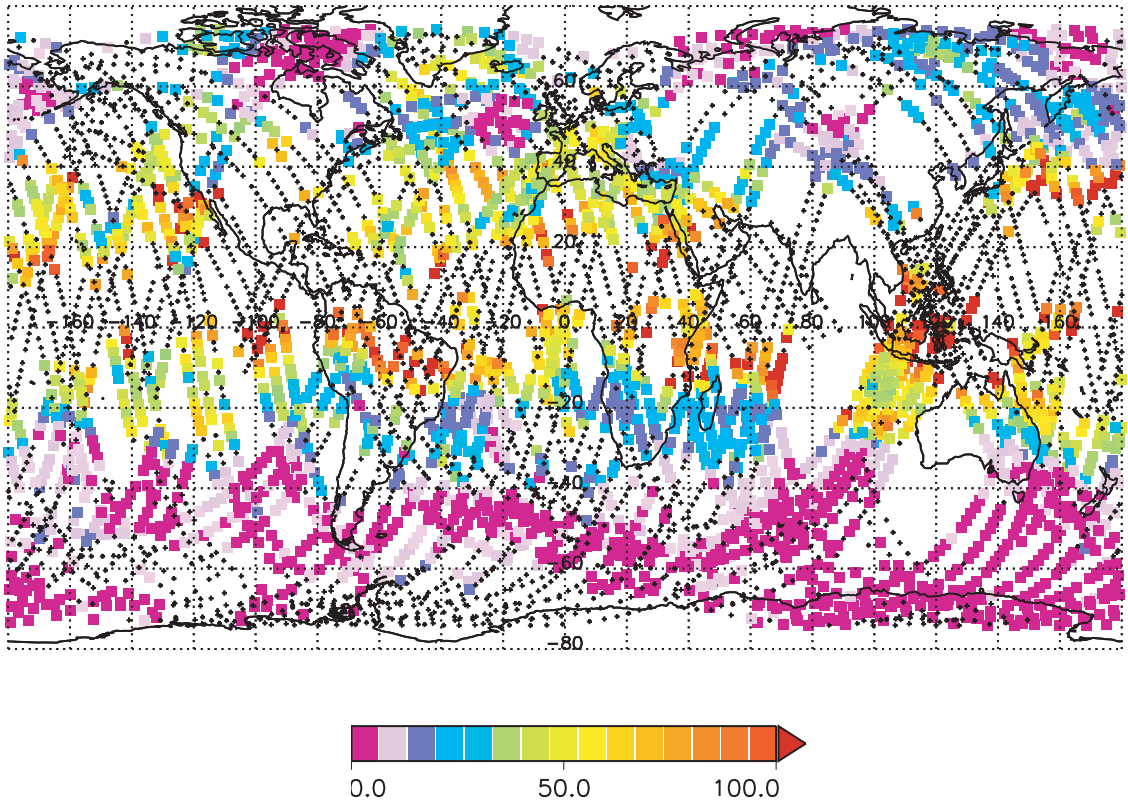

Figure 4. Global map of water vapor volume mixing ratios at 215 hPa altitude. Crosses denote cloud-covered areas, where H_2O retrieval at low altitudes was impossible. Map shows 24 hours of measurements on 11/12 August 1997. Color code gives volume mixing ratios in ppm.

Hygrometer (FISH) [*Zoeger et al.*, 1999] was flown on a Falcon aircraft (of DLR) at and above the tropopause on 5 days of the CRISTA 2 mission in central Europe (several hours per day). During this mission the CRISTA instrument view direction could be pointed in any direction desired ("pointing mode" of the center telescope; for details, see *Offermann et al.* [2001]). During the CRISTA underflights the airplane trajectories were chosen such that they were near to the satellite orbits. In addition the CRISTA view direction was pointed toward the airplane. In this way quite a number of close coincidences of the two types of measurement were obtained. Analysis of these data show some differences, the magnitudes of which strongly depend on the miss-distance. A miss-distance of 200 km is still too large to yield a good data comparison. Miss-time, on the other hand, does not appear to be too important. Measurements differing in time by several hours appear to be acceptable for comparison. As an example Figure 3 shows two scatterplots of the CRISTA (center telescope) and FISH data. Miss-distance is below 50 km in Figure 3a, and miss-time less than 2 hours. Altitude range is 175–225 hPa. FISH data are 1 min mean values. There are 28 FISH values compared to four CRISTA altitude scans in the picture. The vertical columns of data points indicate the atmospheric variability measured by FISH in the neighborhood of one CRISTA point (center of footprint). A close agreement of the two data sets is seen in Figure 3a, with a correlation coefficient of 0.97. The dashed line in Figure 3a is a regression curve with a slope of 1.08 and a "bias" of −2 ppm. In Figure 3b the maximum miss-distance was increased to 200 km. The data scatter is strongly increased. The correlation is, nevertheless, still high (0.93).

[14] The measurement accuracy of FISH is believed to be 4–5% [*Zoeger et al.*, 1999], which is much better than the present CRISTA accuracy estimation. In the present paper we therefore rely on the FISH accuracy and on the comparison in Figure 3a as concerns CRISTA absolute accuracy. CRISTA precision of ±11%, however, is believed to be a trustworthy estimate. The detection limit of the CRISTA measurements is determined by the signal-to-noise ratio. A ratio of one corresponds to a mixing ratio of 0.5 ppm. Maximum mixing ratio retrievable with the spectral element used is about 1000 ppm.

[15] A global map of water vapor distribution at 215 hPa altitude measured on 11/12 August 1997 is shown in Figure 4. Each colored point stands for a vertical profile of water vapor volume mixing ratio. The crosses indicate locations where the retrieval was made impossible by high clouds. Thick clouds are easily identified by CRISTA because the infrared spectrum turns into a gray body spectrum. If very thin clouds are present (e.g., haze), water vapor spectral features (Figure 1) may still be visible, though less pronounced due to enhanced "background" emissions. For cloud detection, *Spang et al.* [2001, 2002] introduced a cloud indicator for the CRISTA measurements, based on two different IR wavelengths. This

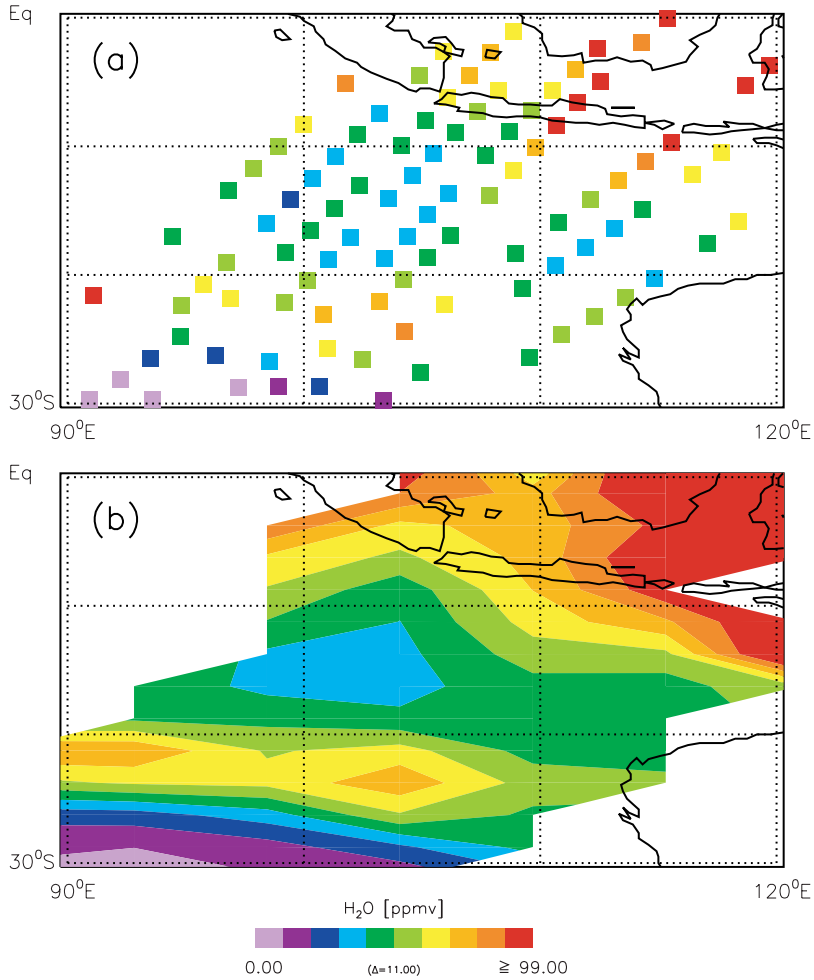

Figure 5. Water vapor volume mixing ratios in the Indonesian area. Altitude is 215 hPa. Data were taken within 3 hours on 11 August 1997. Color code is in ppm. (a) Measured data points. (b) Horizontally interpolated data.

indicator was used here. Details are given by *Schaeler and Riese* [2001].

[16] The color code in Figure 4 shows high values of water vapor in the tropics and subtropics, and a steep decrease to higher latitudes. High variability is seen, even if following the data along an orbital track, where the distance between two points is only 250 km. These differences are believed to be real, taking into account a measurement precision of 11%; the time difference between two measured points is about 0.5 min, only. Very pronounced local structures are seen at many locations on the map. One of them is in the Indonesian area and south of it. Here the CRISTA view directions were specifically pointed during subsequent orbits in a way to substantially increase the measurement density ("Hawk-eye measurement mode") [see *Offermann et al.*, 2001]. In this way the measurement density is increased by a factor of 3–6 and allows this area to be studied in more detail. Respective data are given in Figure 5. In the upper panel the measurement points are shown. In the bottom panel the data have been interpolated horizontally. All data shown were measured within 3 hours on 11 August 1997 (2100–2400 UT). A comparatively dry air mass is seen south of Indonesia with transitions to wet areas further north and south. The northern transition is very steep (factor of two within 1000 km), whereas the southern increase is flatter. There are interesting variations of this structure within a short time frame (less than 1 day). This is discussed below as the structure appears to be typical in space and time.

[17] Relative humidity (RH) has been calculated from CRISTA water vapor mixing ratios, using UK Meteorological Office (UKMO) temperatures [*Swinbank and O'Neill*, 1994]. They show a similarly scattered appearance as the water vapor distribution. This is demonstrated by Figure 6, which shows RH values (RH with respect to ice) at 215 hPa for the whole CRISTA mission. High humidity values are abundant in the tropics as expected. High values, however, are also seen at other latitudes. By the same token low humidity is found in the tropics, too. The Indonesian area shown in Figure 5 is characterized by low humidity in its southern part and by high humidity in the north.

[18] Zonal means of the water vapor data shown in Figure 4 (and the other days of the mission) are given in Figure 7 (upper panel). The error bars do not include the absolute error. The maximum of the distribution is not located at the equator, but somewhat shifted into the summer hemisphere. The latitudinal gradients are mostly strong, with a water vapor decrease of about 3 ppm per degree latitude on its southern flank (5°N–40°S). The standard deviations of the

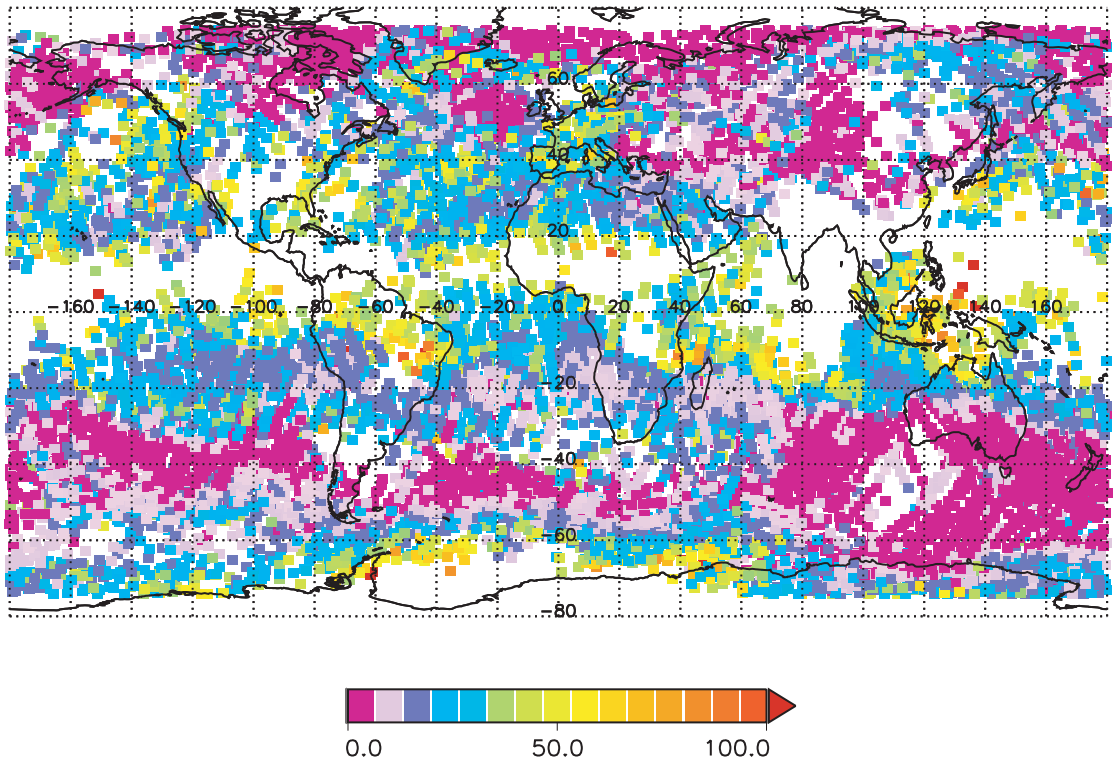

Figure 6. Relative Humudity (RH) with respect to ice measured during the entire CRISTA 2 mission. Altitude is 215 hPa. Humidity is in percent.

means shown in the upper panel are given in the lower panel in percent. These latter values are high, thus quantifying the atmospheric variability mentioned. Several conspicuous maxima and minima appear and these are discussed below (section 3.5).

[19] To study water vapor variability in more detail the fluctuation dependence on the horizontal scale was analyzed. For this purpose the latitude belt 35°–55°N was chosen. Differences of next neighbor CRISTA data points were calculated along orbital tracks, and their standard deviations were determined. The horizontal distance of such points was 250 km, and standard deviations are taken as a measure of the fluctuations on this scale. The same was done for second, third, and fourth neighbors to obtain results for the scales of 500, 750, and 1000 km. Time differences of measurement pairs were less than 4 min. The results are shown for the European sector 0°–20°E in Figure 8 (circles). Fluctuations are high—as already discussed—and show some decrease with horizontal scale. If the longitudinal extent of the latitude belt is not restricted the fluctuations are much larger. This is shown by the crosses in Figure 8.

[20] Data on much smaller scales are available from the FISH measurements. These measurements are taken in situ. They are very fast (1 s per data point), and therefore have small spatial differences. Hence unbiased differences and their standard deviations can be calculated for very small horizontal scales. They are shown in Figure 8 (triangles) down to scales of 200 m. The time difference of these FISH data pairs is less than 25 min. Each triangle is based on several thousand data pairs. The data show a steady decrease of water vapor variability with horizontal scale. They are the mean of five sets of data taken on 5 days. The bar given with the 100 km value indicates the typical standard deviations for these 5 days. The CRISTA data stem from 5 days in the same period, and their scatter (not shown) is very similar or somewhat larger. Hence the good agreement of the two data sets at 250 km may be somewhat fortuitous.

[21] The data in Figure 8 follow a smooth curve. This curve can be approximated in its middle section by a linear fit curve as shown by the solid line. The line is based on the FISH data from 5 to 250 km. It is also approximately representative of the CRISTA data points in the European sector. At scales shorter than 5 km a break appears to occur, and the FISH data suggest a decay about twice as steep.

3. Discussion

3.1. Satellite Intercomparison

[22] The MLS [e.g., *Stone et al.*, 2000; *Read et al.*, 2001] on UARS was the only satellite experiment to take water vapor measurements near the tropopause at high data rate during the second CRISTA flight. A data comparison is therefore performed, and it can be based on a relatively large number of coincidences.

[23] The MLS experiment measures atmospheric emissions in a limb-scanning mode as does CRISTA. CRISTA zonal mean data in Figure 7 are compared to MLS climatology data taken from the work of *Read et al.* [2001]. Version 4.9 data of MLS are used, representing the June–August period of years 1991–1997. (This time interval does

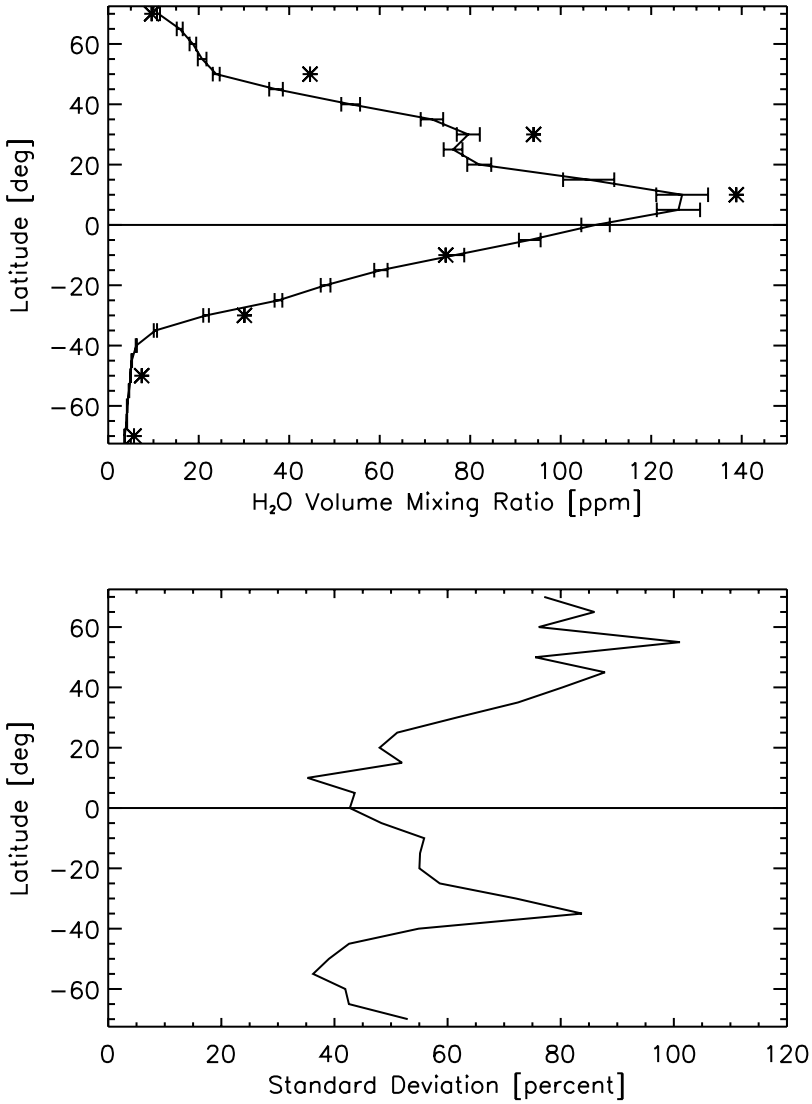

Figure 7. Zonal means of water vapor mixing ratios at 11.5 km altitude measured during the mission (upper panel). Standard deviations of the data are given in the lower panel. Asterisks show MLS Version 4.9 data for comparison.

not include the CRISTA 2 mission, as Version 4.9 data are no longer available after June 1997.) The absolute error of the Version 4.9 data as taken from the work of *Read et al.* [2001, Table 1] for 215 hPa is about 22%. The CRISTA and MLS Version 4.9 data thus agree far better than within their combined errors. The CRISTA data are systematically a little lower than the MLS climatology.

[24] The UARS satellite was pointed southward during the second CRISTA mission, and therefore water vapor data of MLS and CRISTA can only be directly compared south of 34°N. Measurement coincidences are shown in Figure 9 with miss-distances smaller than 200 km and miss-times less than 2 hours. Version 5 data of MLS are used in this picture. Figure 9 shows a large scatter of the data (note the logarithmic scales). The dashed curve in Figure 9 was drawn parallel to the diagonal and in such a way that half of the data points lie above it, and half below. It is by a factor of about 0.67 below the diagonal, suggesting a dry bias of MLS Version 5 data against CRISTA. The bias would be increased if the CRISTA data were corrected upward to make them better agree with MLS Version 4.9 data in Figure 7.

[25] When discussing this difference the following needs to be taken into account: After June 1997 the temperature/pressure radiometer of MLS had to be shut off because a battery on UARS failed. MLS upper tropospheric humidity (UTH) data processing was impacted by this. Version 4.9 data are no longer available, and are replaced by Version 5.0 data (N. J. Livesey et al., The UARS MLS version 5 data set: Theory, characterization, and validation, submitted to *Journal of Geophysical Research*, 2001). For test purposes the modified Version 5 algorithm was run on data taken prior to June 1997 and compared with UTH data from the Version 4.9 algorithm. Same day comparisons of UTH between Version 4.9 and ''post-June 1997'' Version 5 algorithm reveals that the Version 5 UTH is drier than Version 4.9. The exact relation is beyond the scope of the present paper, which has its emphasis on relative variations rather than absolute values. It should also be noted that the

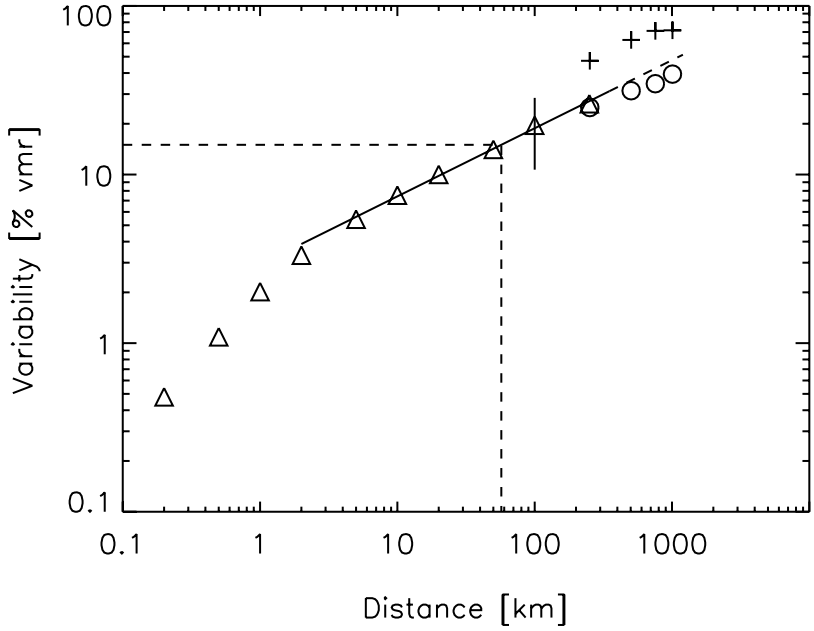

Figure 8. Water vapor variability versus horizontal scale. Standard deviations of volume mixing ratio differences at various distances are given in percent. Altitude is 12.5 km and latitude band is 35°–55° N. CRISTA data are given by circles and crosses and FISH data are given by triangles (see text).

CRISTA data shown in Figures 7 and 9 were derived using UKMO temperatures, whereas NCEP temperatures were used for the MLS data. In case there is any bias between these two temperature sets, the data comparison in the two figures would be affected [*Read et al.*, 2001, section 4.1].

[26] The data scatter in Figure 9 comprises the instrumental noise of the two experiments as well as the atmospheric variability. It is not easy to disentangle these three factors. An attempt to estimate them, however, can be made by using an "Eigen-scatterplot" as shown in Figure 10a: CRISTA data are plotted versus CRISTA data in a scatter diagram similar to Figure 9 (coordinate scales are the same). Miss-time is 2 hours as before. Miss-distance was, however, increased to 400 km. This was done to obtain a sufficient number of data points in the case of Figure 10b, which shows the same Eigen-scatterplot for MLS. To keep the number of data points comparable in Figures 10a and 10b only one telescope of CRISTA is used in Figure 10a (center

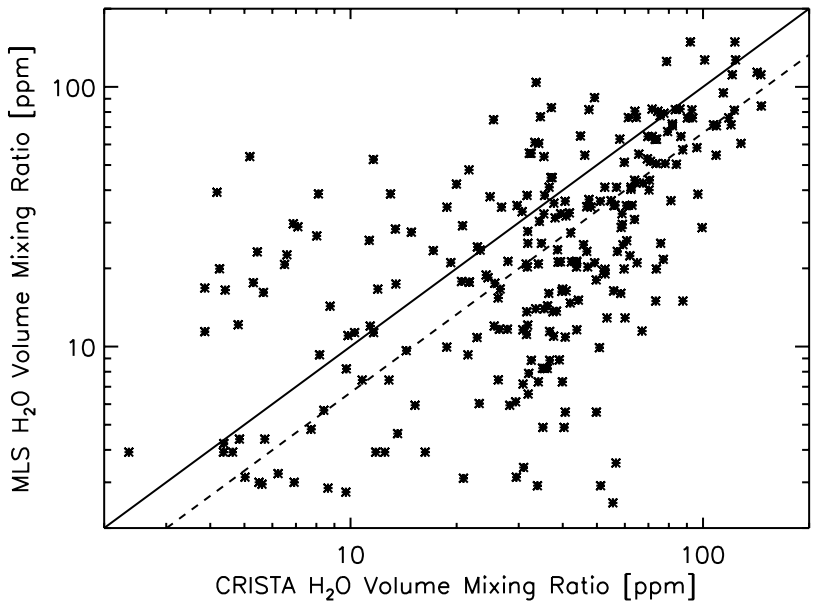

Figure 9. Coincidences of CRISTA and MLS water vapor measurements. Altitude is 215 hPa, miss-distance is less than 200 km, and miss-time less than 2 hours. MLS data are Version 5.0. In total, 262 coincidences are shown. Dashed curve is by a factor 0.67 below the diagonal (see text).

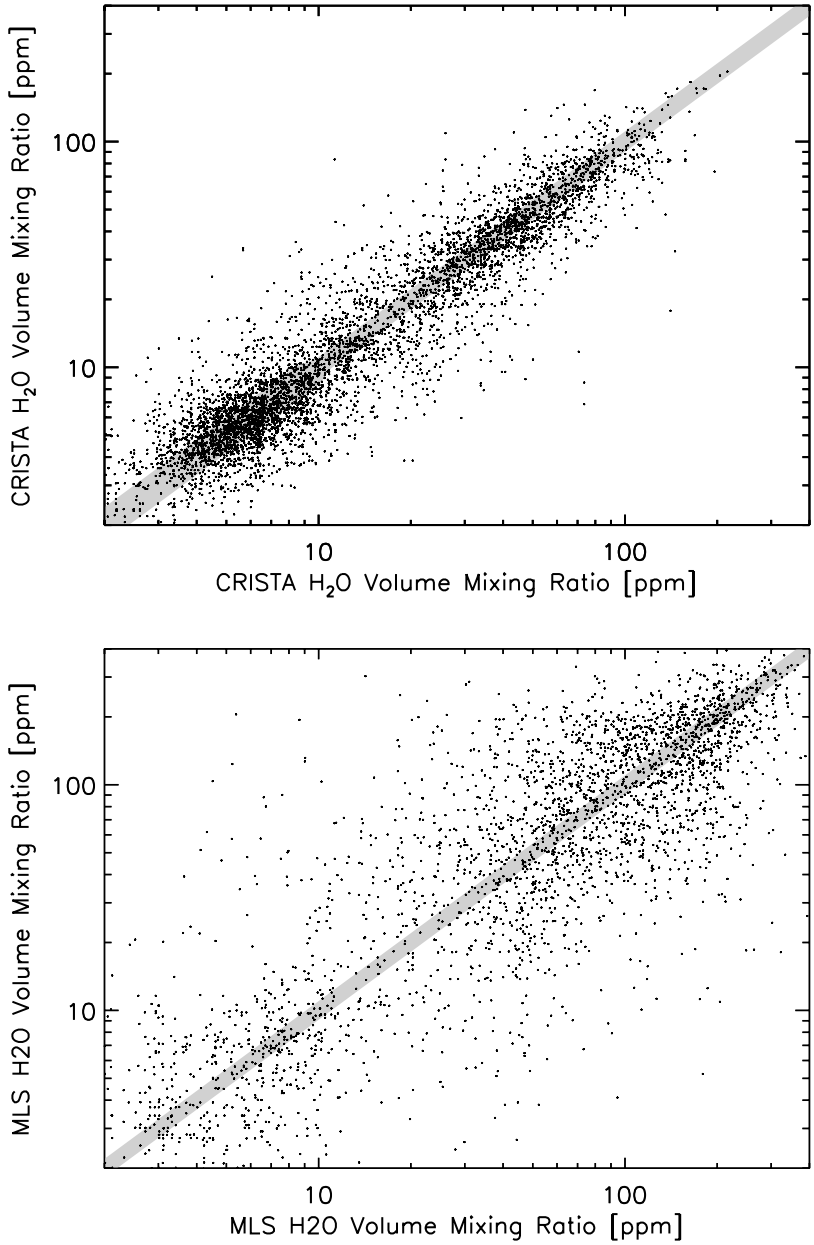

Figure 10. Water vapor "Eigen-scatter" diagrams. (a, top) CRISTA versus CRISTA. (b, bottom) MLS versus MLS. Altitude is 215 hPa. Miss-distance is less than 400 km and miss-time is less than 2 hours. Shaded areas along the diagonals indicate the noise of the instruments. MLS data are Version 5.0. Only one CRISTA view direction is used (see text).

telescope). The data points are from the time interval of the entire CRISTA mission. The atmospheric contribution to the scatter in Figure 10 should have increased by a substantial factor as compared to Figure 9 because of the increase in miss-distance (see Figure 8). The shaded area around the diagonal of Figure 10a indicates the CRISTA instrumental noise of ±11%. (At small signals this increases to ±20%.) The remainder of the scatter is believed to be of atmospheric origin. (It should be remembered that a standard deviation if estimated from the scatter in Figure 10a would be somewhat different from the fluctuations of the first-order differences given in Figure 8. It would be smaller by a factor $\sqrt{2}$ if the data are uncorrelated. Difference in miss-time also should have some influence).

[27] The shaded area in Figure 10b is the noise of the MLS Version 4.9 data (±10%) taken from the work of *Read et al.* [2001]. The data scatter in Figure 10b is considerably larger than that in Figure 10a (same coordinate scales). It must therefore be concluded that the MLS Version 5 data have some additional noise. This might in part be due to the much larger field-of-view of MLS (MLS: 4 km, CRISTA < 1.5 km).

[28] If the horizontal water vapor distribution of CRISTA (Figure 4) is compared to a respective map of MLS data several points are noticed:

1. The pronounced structures in the water vapor field at middle and high northern latitudes in Figure 4 cannot be checked by MLS because the UARS satellite was south looking at this time.

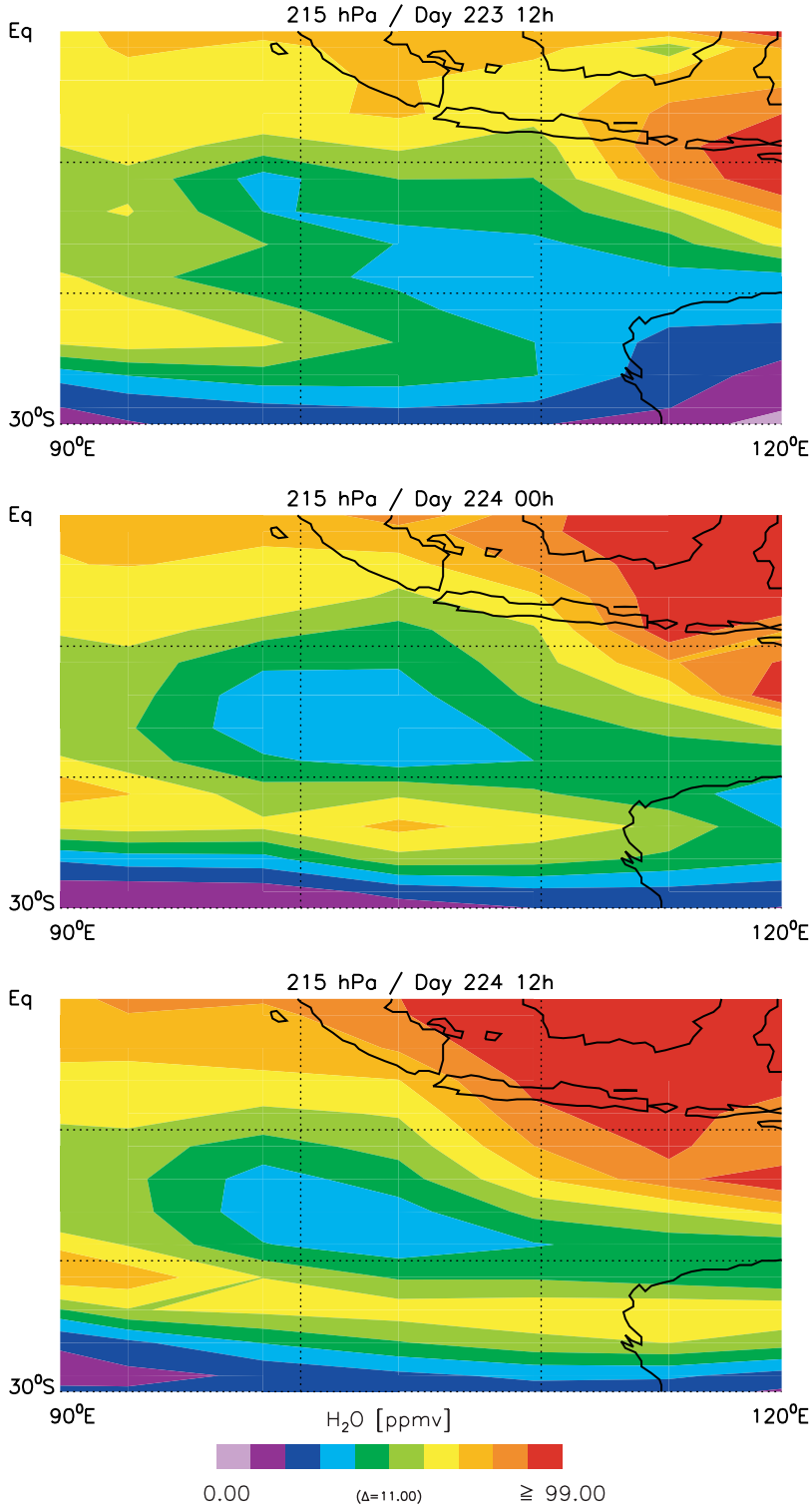

Figure 11. Entrapment of a dry air parcel by moist air south of Sumatra. Color code gives volume mixing ratios in ppm. Assimilated water vapor data are shown at time steps of 12 hours (top: 1200 UT on 11 August 1997, middle: 0000 UT on 12 August 1997, and bottom: 1200 UT on 12 August 1997). Altitude is 215 hPa, latitude 0°–30°S, and longitude 90°–120°E.

2. Small-scale structures as that shown in Figure 5 and in Figures 11 and 12 (see below) can only be identified by CRISTA because a high data density is needed.

3. There are large areas in the tropics, and also at other latitudes, where water vapor is not available from CRISTA because of high clouds. MLS water vapor data, on the other hand, are at hand at all of these places. A joint interpretation of these two complementary data sets appears therefore rewarding. It is, however, beyond the scope of this paper.

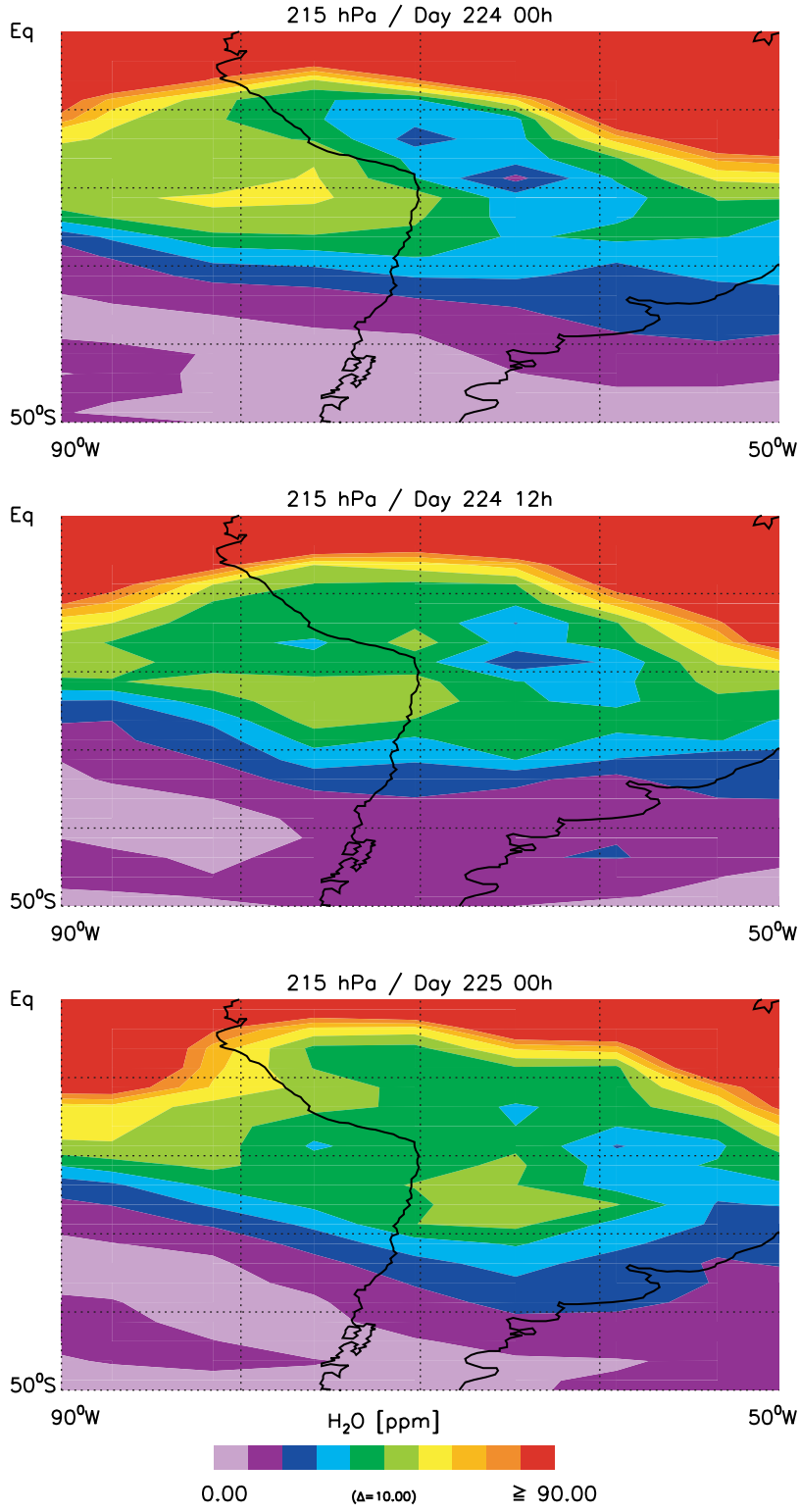

Figure 12. Separation of a wet air parcel from the tropics near Peru/Chile. Color code gives volume mixing ratios in ppm. Assimilated water vapor data are shown for 24 hours on 12 August 1997 (top: 0000 UT, middle: 1200 UT, and bottom: 2400 UT). Altitude is 215 hPa, latitude 0°–50°S, and longitude 50°–90°W.

3.2. Water Vapor Variability

[29] The most pronounced feature of the data presented here is their high variability. The horizontal distribution of the water vapor shows a patchy structure, and it appears not unreasonable to assume a cloud-like appearance of wet and dry air parcels. It would be interesting to know the typical scales of these parcels/air masses, for instance for climate studies.

[30] An estimate of this scale can be obtained from the mean correlation length L

$$L = \int_{\circ}^{\infty} r(x) \cdot dx \tag{1}$$

where x denotes the horizontal distance, and r is the correlation coefficient. The data shown in Figure 8 can be used for a respective estimate. The standard deviation $\sigma(x)$ of the differences of neighbors at a distance x in a data series can be related to the autocorrelation coefficient of the data series by

$$\sigma^2(x) \approx 2 \cdot \sigma_0^2[1 - R(x)] \tag{2}$$

Here $R(x)$ denotes the autocorrelation coefficient for lag x, and σ_0^2 is the variance of the whole data set. Equation (2) is only approximately valid because the measurement series used here are relatively short. The σ_0 value for the CRISTA data shown in Figure 8 for the 0–20°E area is about 28%. Entering this into equation (2) and using σ(x) from Figure 8, the autocorrelation function $R(x)$ can be derived. If $r(x)$ and $R(x)$ can be assumed to be approximately the same, a correlation length of about 400 km is obtained from equation (1).

[31] The fit line in Figure 8 (5–250 km) indicates a scaling behavior: if the standard deviations given are squared, a second-order structure function is obtained [*Cho et al.*, 2000]. The fit line is thus transformed into another straight line with double gradient. A slope of 0.81 is obtained this way. This procedure was repeated separately for the five airplane data sets. The standard deviation of the slopes obtained is ±0.01, which may be considered as an error estimate for the slope, following the work of *Cho et al.* [2000]. These authors obtain a slope of 0.79 ± 0.05 in the extratropical free troposphere at similar horizontal scales. This value is near to our result of 0.81 ± 0.01, which stems from somewhat higher altitudes. Further structure functions from MOZAIC and ER2 measurements are presented by *Kley et al.* [2000]. The slopes appear to be similar to those reported here. A more detailed analysis of our data is thus suggested. It is, however, beyond the scope of the present paper.

[32] The large variances of water vapor mixing ratios suggest some speculations about their origin. If transports should be a reason, those in the vertical direction lend themselves to an explanation because of the steep gradient of water vapor near the tropopause. *Pfister et al.* [1993] suggest convective systems as the origin of gravity waves in the tropics. Vertical displacements of ±200 m (or somewhat less) are discussed in connection with horizontal scales of 50–100 km. The vertical water vapor gradient in Figure 2 is about 7.4% change per 100 m. A ±200 m displacement thus means about a ±15% change of water vapor mixing ratio. Using Figure 8 this variation is related to a horizontal disturbance of 57 km, which is on the order of *Pfister et al.* [1993]. It may therefore be concluded that at least part of the distribution shown in Figure 8 might be related to convectively generated gravity waves. (The value of 57 km is an approximate one considering the scatter bar in Figure 8. It has furthermore been assumed here that the distribution shown in Figure 8 for northern midlatitudes is approximately valid in the tropics, too.)

[33] The high water vapor variability has practical consequences for instrument intercomparisons. It implies that quite a number of measurements are necessary to make an intercomparison statistically significant. Given an intercomparison at miss-distance of $\leq$50 km and a miss-time less than 25 min, Figure 8 predicts an atmospheric standard deviation of 14%. If, for instance, the high accuracy of the FISH instrument is to be exploited in such a comparison, the total statistical error must be less than 4%. The number of intercomparison measurements therefore must be larger than $\left(\frac{14}{4}\right)^2 = 12.25$. Respective requirements apply to and are fulfilled for the FISH–CRISTA intercomparison of Figure 3a.

3.3. Relative Humidity

[34] RH is shown in Figure 6 as measured during the entire CRISTA mission. The distribution is strongly structured on the horizontal in the same way as the water vapor in Figure 4. It is qualitatively similar to what was found from MLS measurements during the summer by *Jensen et al.* [1999] at a somewhat higher altitude and by *Read et al.* [2001] at the same altitude.

[35] Occurrence of supersaturation (RH > 100%) is of interest, especially for microphysical and climatological reasons. A statistical analysis of the RH values in Figure 6 was therefore performed for the tropics (±20° latitude). Very low occurrence rates of supersaturation were found (less than one percent). They are compared to data from the Measurement of Ozone and Water Vapor Airbus In-Service Aircraft (MOZAIC) [*Marenco et al.*, 1998; *Helten et al.*, 1998, 1999]. These data were taken during the CRISTA period. Occurrence rates are much higher (14.4% at 215 hPa) than the CRISTA results.

[36] There may be several reasons why the CRISTA supersaturation occurrence is so much smaller than that of MOZAIC. A major factor could be the difference in sensing volume of the two measurement techniques. MOZAIC as an airplane in situ measurement senses a volume of about 10 km along track (1 min data) and almost zero extension across track and in the vertical. Contrary to this the air volume sensed by CRISTA is less than 150 km in the view direction, 20 km across this direction, and less than 0.5 km in the vertical. Hence if a supersaturated air mass diameter is of the order of 150 km, and/or its thickness of the order 0.5 km its signal would be smeared by the CRISTA measurement, i.e., the detection probability would be decreased. To obtain reliable statistics it is necessary that the dimensions of the supersaturated air mass be much larger than those of the measurement volume. The approximate horizontal correlation length L of water vapor derived from Figure 8 is 400 km. A similar order of magnitude is assumed here for the size of the RH distributions. *Gierens and Spichtinger* [2000] obtain a somewhat smaller "mean path length" of 150 km. These scales are much larger than

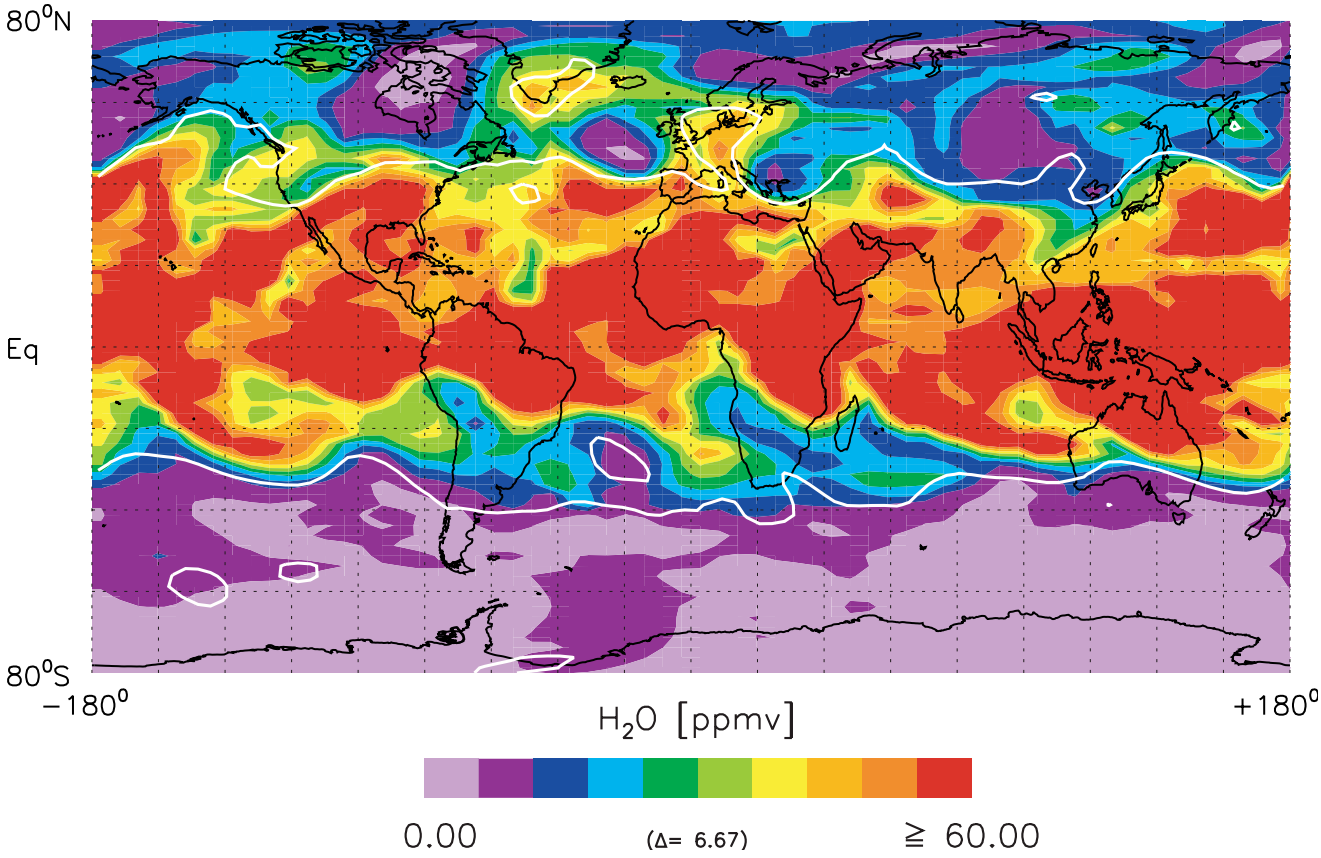

Figure 13. Assimilated water vapor data at 215 hPa altitude on 12 August 1997. Color code gives volume mixing ratios in ppm. White lines indicate the tropopause (2.5 PV units taken from UKMO). For details, see text.

the 10 km scale of the MOZAIC measurement. Hence the above condition is obviously fulfilled for the MOZAIC experiment. This is not the case for CRISTA. The scales are of the same order of magnitude as the length of the CRISTA footprint, i.e., the CRISTA sensing dimension in the horizontal appears to be too large. A similar conclusion applies for the vertical direction. Vertical extension of supersaturated regions could be as small as 0.5 km, as a vertical uplift of about 0.5 km is frequently sufficient to cool the air to the level required for supersaturation [*Gierens et al.*, 1999]. Vertical thickness of cirrus clouds is frequently around 0.5 km, and thus points in the same direction [e.g., *Winker and Trepte*, 1998]. In summary there are doubts about the suitability of CRISTA for supersaturation probability analyses. This may also apply to other experiments using similar limb-viewing geometries.

[37] It should be noted that the CRISTA RH values were calculated by means of UKMO temperatures. If these temperatures should have a bias (as discussed, for instance, by *Keil et al.* [2001] for higher altitudes) the present results and consequences would be directly affected. A warm bias with respect to the MOZAIC temperatures, for instance, would lead to decreased occurrence rates found by CRISTA.

3.4. Data Assimilation

[38] To study the small-scale structures in further detail the measured water vapor mixing ratios were assimilated by a three-dimensional chemical transport model. A sequential trace-gas assimilation technique described by *Riese et al.* [1999b] was used, which utilizes the transport code of the NCAR ROSE model [e.g., *Rose and Brasseur*, 1989; *Smith*, 1995]. The model is driven by analyzed wind and temperature fields provided by the UKMO [*Swinbank and O'Neill*, 1994]. The system has been used in previous studies [e.g., *Riese et al.*, 1999b; *Riese et al.*, 2000] in combination with the chemistry package of ROSE. In the present analysis the vertical wind components of the UKMO wind field was found unreliable (much too high occasionally). Vertical winds of (almost) zero strength were therefore chosen as a first approximation here. The results of the H_2O assimilation are shown in Figure 13 for an altitude of 215 hPa on 12 August 1997. The picture shows a highly structured water vapor distribution especially in the tropics and subtropics. The white lines are isolines at 2.5 PV units, i.e., approximately indicative of the tropopause (following the work of *Haynes and Shuckburgh* [2000]). The resolution of the assimilated H_2O fields shown is 2.5° in latitude and 5.6° in longitude. Hence it is relatively coarse as—for instance—compared to the small scales seen in Figure 5. Nevertheless it is sufficient to show the water vapor minimum south of Indonesia. This minimum appears to indicate a dry air mass that is encircled and trapped by wet air. Figure 13 shows several other locations at similar latitudes with dry air masses in different stages of such entrapment. The reverse process

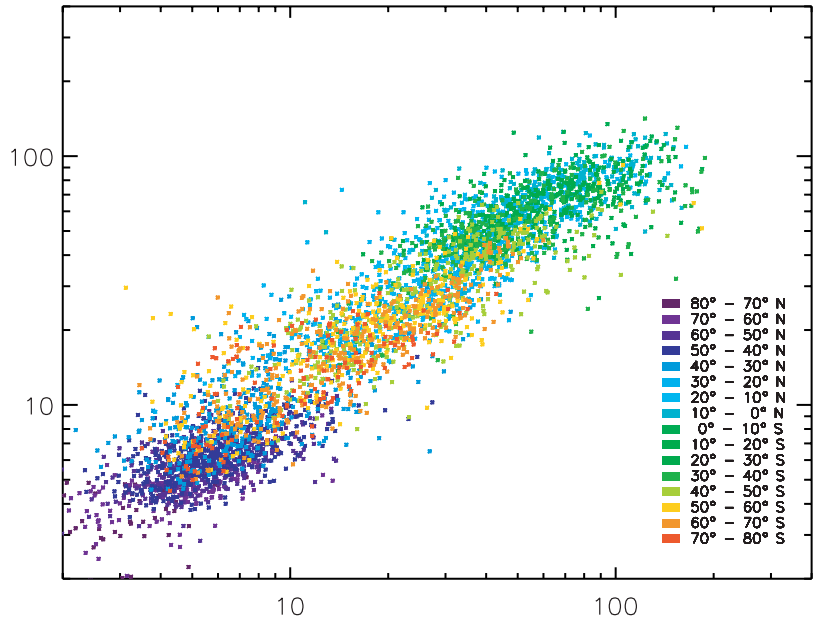

Figure 14. Scatterplot of assimilated versus measured water vapor mixing ratios at 215 hPa altitude on 12 August 1997. Correlation coefficient is 0.87. Color code gives latitude bands in 10° steps.

also appears to occur, i.e., wet air masses separate from the subtropics and drift away (e.g., at the west coast of South America). Similar structures are present in the northern hemisphere.

[39] To test the reliability of these model results we have tried to validate the H_2O distributions obtained from the assimilation. For this purpose Figure 14 shows a scatterplot of the forecast of the assimilation system at the locations and times of the observations versus the water vapor mixing ratios observed by CRISTA. Data are for 12 August 1997 at an altitude of 215 hPa. They show a fairly large scatter. If the data of Figure 14 are plotted in a horizontal map (not shown here) the distribution of high and low differences appears to be at random. It is in agreement with this finding that the color code of Figure 14 does not reveal a latitude dependence of the differences.

[40] Part of the scatter seen in Figure 14 is due to the high miss-time of the data pairs. As model forecasts are compared to measurements here, this miss-time is typically 12 hours. The differences shown are therefore conservative upper limits. Another reason for the scatter is presumably the spatial model resolution used for the assimilation. It is of the same order as the miss-distance used for the Eigen-scatter analysis in Figure 10a. The scatter in Figures 10a and 14 is fairly similar. It is believed that a calculation with finer resolution may considerably reduce this scatter as this is the case if the miss-distance in the Eigen-scatter analysis is chosen smaller (see also Figure 8). Such calculations at finer resolution as well as refined initialization procedures will be tested in future analyses. The slight bias between assimilated and measured data at high H_2O values (see Figure 14) is mainly due to the model initialization (1 August 1997), which is currently based on zonally averaged CRISTA observations.

[41] To further check upon the assimilated data they are compared to the independent FISH data in Figure 15. In this scatterplot the miss-distance is less than 50 km, and the miss-time is less than 2 hours to make the plot comparable to Figure 3a. (Data $\geq$ 10 ppm are used, only.) A close correlation between the measured and the assimilated data is found, with a correlation coefficient r = 0.99. A least squares fit to the data in Figure 15 is similar to that in Figure 3a (slope 1.22, "bias" −6 ppm). In summary the assimilated data appear quite reliable, and can be used for flux studies and possibly for stratosphere–troposphere exchange analyses in the future.

[42] Such studies are beyond the scope of the present introductory paper. The assimilated data can, however, be used to demonstrate the nature of these processes and estimate the order of magnitude of such fluxes in the subtropics in a simple way. In Figure 5 a trough of low water vapor mixing ratios is seen south of Indonesia. The development of this peculiar structure can be followed in the assimilated data. Figure 11 shows three stages of the assimilated water vapor in this geographical area, at time steps of 12 hours. A tongue of moist air develops, which tends to encircle the dry air south of Sumatra. In the last picture (bottom of Figure 11) this air mass appears to have been almost entrapped by the moist air. (Note the similarity of Figures 11b and 5b.) There are several structures of this kind in Figure 13 at southern and northern subtropical latitudes. The time development of some of them indicates that after (or during) the trapping of a dry air mass an adjustment of its humidity and of that of the surrounding air occurs. This can possibly be interpreted as an equatorward mixing event. There are also several events indicated in Figure 13, where moist air masses appear to be transported in the opposite direction. An example is given in Figure 12. It shows a relatively wet air mass west of and above Peru and Chile over a time period of 24 hours. It travels slowly southeastward and thereby apparently has a tendency to separate from the tropics.

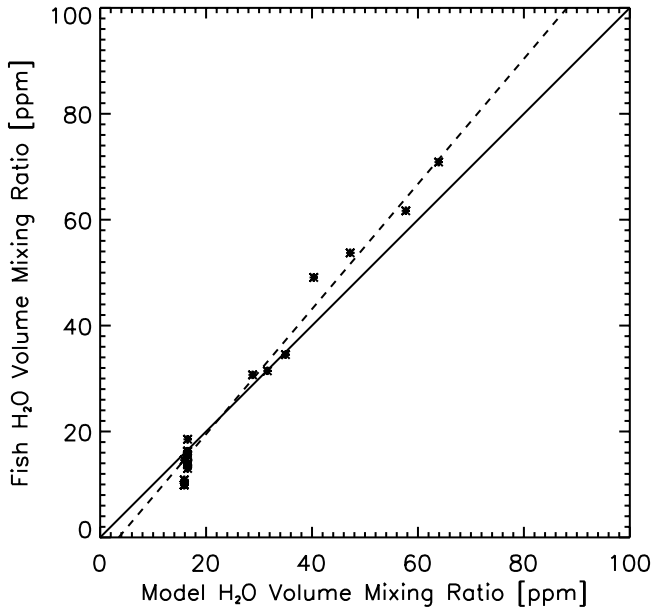

Figure 15. Scatterplot of water vapor mixing ratios measured by the FISH experiment versus assimilated CRISTA data. Altitude is 150–215 hPa, miss-distance is less than 50 km, and miss-time less than 2 hours. Data are from 11 to 13 August 1997. The number of data points is 20.

Figure 13 (and the maps on the days before and after, not shown here) thus suggest considerable bidirectional meridional transport, which may include stratosphere–troposphere exchange.

3.5. Atmospheric Diffusivity

[43] The large variability of water vapor mixing ratio is believed to be mostly due to transports on various scales. Small horizontal scales have recently been analyzed in a comprehensive study by *Haynes and Shuckburgh* [2000] in the lowest stratosphere and upper troposphere. These authors determine an atmospheric effective diffusivity K_{eff} on the basis of the work of *Nakamura* [1996] using ECMWF meteorological data. The K_{eff} values they obtain strongly depend on latitude and altitude. This can be compared to the CRISTA data presented here.

[44] The time development of air parcels such as those shown in Figures 11 and 12 can be used to estimate the order of magnitude of meridional trace-gas transports. The typical timescale of a "mixing event" described above appears to be 2–3 days. A typical scale in the latitudinal as well as the longitudinal direction appears to be on the order 1000–2000 km. Using the mean values and taking into account that about five events occur simultaneously along a latitude circle in Figure 13 the effective meridional transport velocity is 1.3 m/s. Multiplying this by the meridional scale provides an order of magnitude estimate of the eddy coefficient K_e, giving a value of about $K_e = 2 \cdot 10^6 \frac{m^2}{s}$. This is almost the same as the effective diffusivity that Haynes and Shuckburgh (their Plate 2) obtain at the 330–350 K levels in the summer months (June–August). The close agreement is, of course, fortuitous. We may, however, conclude that the same order of magnitude is arrived at by our rough estimation, and that a more quantitative comparison of fluxes by means of the assimilated H_2O data could be rewarding in a future analysis.

[45] A somewhat closer K_{eff} comparison can be made by means of the data shown in Figure 7. In the top part of this picture, water vapor zonal means are shown. In the bottom part the corresponding standard deviations σ are given (in percent). These σ values show a pronounced latitudinal structure, which appears difficult to understand at first glance. It can be elucidated, however, by a comparison with the effective diffusivities K_{eff} of Haynes and Shuckburgh. These diffusivities apply to zonal belts by nature, as do the σ values in Figure 7. The effective horizontal diffusivities show considerable variations with latitude, too [*Haynes and Shuckburgh*, 2000, Plates 1 and 2]. In an approximation it may be assumed that the fluctuation of the water vapor mixing ratio μ is proportional to the horizontal transport scale L

$$\sigma \approx \frac{\partial \mu}{\partial x} \cdot L \tag{3}$$

Here σ is the standard deviation of μ and represents the fluctuations of μ. $\partial\mu/\partial x$ is the horizontal gradient of the water vapor mixing ratios. Squaring equation (3) and extending by the timescale τ we get

$$\sigma^2 \approx \left(\frac{\partial \mu}{\partial x}\right)^2 \cdot \tau \cdot K_e \tag{4}$$

where K_e is the horizontal eddy coefficient $\frac{L^2}{\tau}$. Hence a proportionality between the effective diffusivities K_{eff} of Haynes and Shuckburgh and the measured water vapor variances could be expected in this approximation if the timescale τ does not vary too much. The K_{eff} values of Haynes and Shuckburgh are therefore taken from their Plate 2 for the 340 K level in summer (June–August) and replotted in Figure 16 (solid line). They are compared to the water vapor variances as calculated from Figure 7 (dotted line). It should be noted that K_{eff} is an amplification factor over a basic and somewhat arbitrary global atmospheric diffusivity [see *Haynes and Shuckburgh*, 2000]. Hence the K_{eff} scale in Figure 16 is a relative one and was chosen so that the two curves are best comparable. The K_{eff} values are given for equivalent latitudes by Haynes and Shuckburgh. The CRISTA data are in geographic coordinates (Figures 7 and 16). To take this difference into account—at least approximately—the K_{eff} values were shifted southward by about 18°. This was motivated by the fact that—according to the season—the zeroline of the potential vorticity was displaced southward from the equator (by more that 20° in places; the shift of 18° was chosen such that optimum agreement of the two curves in Figure 16 is obtained). The similarity of the two curves in Figure 16 is quite interesting, if their pronounced structures are considered. Some of these have been discussed by *Haynes and Shuckburgh* [2000]. Following their analysis the three minima in Figure 16 have been numbered and are identified as the following transport barriers: 1: southern tropopause barrier; 2: lower tropical barrier; 3: northern tropopause barrier. This latter barrier is not very pronounced, and its exact location is dubious at this time of the year.

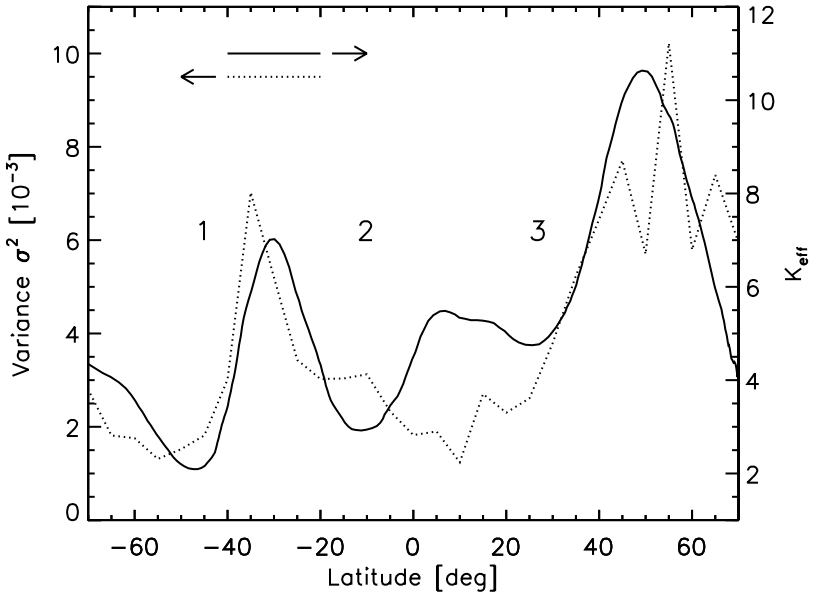

Figure 16. Water vapor variance σ^2 as compared to effective eddy diffusivity K_{eff}. Variances are derived from Figure 7 and are given as a dotted line (left scale). Eddy coefficients (solid line, right scale) are taken from the work of *Haynes and Shuckburgh* [2000] for the 340 K isentropic level. For details and discussion of the numbered minima, see text.

[46] The close agreement between data variance and effective diffusivity in Figure 16 is quite surprising considering the coarse assumptions made for equation (4). It suggests a quantitative comparison of trace-gas fluxes in the future, as said above. There is a disagreement between the two curves at 0–20°N, which also needs to be analyzed.

4. Summary and Conclusions

[47] During the second CRISTA mission (7–19 August 1997) the altitude range of the measurements was extended downward such that it reached well below the tropopause in most parts of the globe. The CRISTA instrument uses IR spectrometers that scan the infrared spectral range from 4 to 14 μm almost without gaps. Therefore a water vapor emission feature was sought—and found—in this spectral range, which is suitable for water vapor retrieval at low altitudes (12.7 μm). Two other spectral element were used to determine high clouds (12.0 and 12.6 μm). At the locations of high clouds or cirrus, water vapor cannot be retrieved. This data loss is, however, tolerable at most latitudes.

[48] The helium cooling of the CRISTA instrument enables a high measurement speed, which translates into a close distance of each two subsequent measurement points along orbit track (250 km). At the same time the detector noise is small. In combination with the high accuracy of the view direction a good measurement precision is obtained (11%). The high point density along track together with the threefold view directions of CRISTA yield a high data density that has not been achieved by any limb-scanning instrument before. This density was even increased at certain locations by applying a special ("hawk-eye") measurement mode. A mean distance of data points of about 165 km was achieved here. Hence CRISTA is especially suited for the study of the high variability in space and time of water vapor in the upper troposphere.

[49] The only satellite experiment that took measurements at high data rate simultaneously with CRISTA was MLS on UARS. We compare CRISTA with two data products: the MLS Version 4.9 climatology, and Version 5 coincident data. CRISTA zonal mean data show a very encouraging agreement with the Version 4.9 climatology, which is much closer than the combined error bars. Single CRISTA measurements are compared to respective MLS data at small miss-distances and miss-times (200 km, 2 hours). Smallness of differences is possible because of the high CRISTA data density. MLS Version 4.9 data are not available for this, and Version 5 data have to be used instead. A fairly large dry bias of the MLS Version 5 data with respect to CRISTA is obtained, and additional noise is evident in this data product. The systematic differences between the two MLS data products are presently being analyzed elsewhere. It also still needs to be determined whether the relatively higher MLS noise is due to its much larger field of view (MLS: 4 km, CRISTA < 1.5 km) and/or to other factors.

[50] RH was calculated from the CRISTA data, using the UKMO temperatures. They were analyzed for the occurrence of RH supersaturations. The probabilities obtained are much smaller than those of (nearly simultaneous) MOZAIC data. This may be attributed to the fact that the size of the atmospheric volume sensed by the CRISTA limb scanner is comparable to or large than that of the air volumes with supersaturation. This impedes the detection of supersaturated air parcels. In consequence it appears that limb-scanning instruments may have limitations when RH supersaturation statistics are being derived. The results of the comparison would be different, however, if the UKMO temperatures were to have a bias with respect to the MOZAIC temperatures.

[51] The most striking feature of the global CRISTA water vapor data is their variability: it is very large on all scales accessible to the measurements. On the smallest scales the CRISTA data are (regionally) complemented by airplane in situ measurements (FISH) that extend down to scales well below 1 km. CRISTA global data are taken on a daily basis. They show considerable day-to-day variations especially on the small horizontal scales. Satellite instruments with less data density than CRISTA will have difficulty identifying such structures, as superposition of the data from several days will smear the structures.

[52] The water vapor variability can be analyzed in two ways: (1) as local or regional structures, and (2) on a statistical basis. Pronounced horizontal local structures are ubiquitous. They can be studied especially well by means of the hawk-eye measurement mode. Their variations in time are fast, and therefore considerable horizontal/meridional transports are indicated. The high data density of CRISTA enables a sequential water vapor assimilation that is quite successful. This assimilation scheme is suitable for analysis of the fast variations mentioned. It appears also to be suitable for future detailed transport studies, possibly including stratosphere/troposphere exchange.

[53] A statistical analysis of water vapor spatial variability down to the smallest scales and up to well above 1000 km shows a strong fluctuation increase with spatial scale. The fluctuations indicate a scaling behavior. A structure function is obtained with an exponent of 0.81. This is quite close to the few results presently available in the literature. A mean horizontal extension (correlation length) of water vapor patches is estimated from these data, and is found to be on the order of 400 km.

[54] A diffusion approach is also tried in analyzing the water vapor fluctuations. Respective variances in zonal belts are analyzed for meridional variations. Due to the high data density of CRISTA, very narrow belts (5°) can be chosen. Surprising meridional structuredinal variations of effective eddy diffusivities that were recently presented by *Haynes and Shuckburgh* [2000] and interpreted in terms of transport barriers. Detailed calculations of trace-gas fluxes and eddy coefficients can—and will—be performed by means of the assimilated water vapor fields. This is, however, beyond the scope of the present introductory paper.

[55] The geographical distribution of water vapor fluctuations has, of course, important consequences for the design of any suborbital measurement campaign planned for the validation of satellite instruments.

[56] **Acknowledgments.** We thank M. Schoeberl who encouraged/enabled the low-altitude CRISTA measurements and MLS intercomparison. We also thank G. Brasseur and X. Tie for providing the NCAR ROSE model. We acknowledge the data made available by the MOZAIC program. We are grateful to the Editor and two anonymous referees for many helpful comments and discussions. The CRISTA project is funded by the Bundesministerium für Bildung und Wissenschaft, Bonn, through the Deutsches Zentrum für Luft- und Raumfahrt e.V. (DLR), Bonn, under grant 50 QV 9802 4. The CRISTA and ASTROSPAS instrument was flown by NASA on Space Shuttle mission STS 85.

References

Abbas, M. M., et al., Seasonal variations of water vapor in the lower stratosphere inferred from ATMOS/ATLAS-3 measurements of H_2O and CH_4, *Geophys. Res. Lett.*, *23*, 2401–2404, 1996.

Chen, P., Isentropic cross-tropopause mass exchange in the extratropics, *J. Geophys. Res.*, *100*, 16,661–16,673, 1995.

Chiou, E. W., M. P. McCormick, and W. P. Chu, Global water vapor distributions in the stratosphere and upper troposphere derived from 5.5 years of SAGE II observations (1986–1991), *J. Geophys. Res.*, *102*, 19,105–19,118, 1997.

Cho, J. Y. N., R. E. Newell, and G. W. Sachse, Anomalous scaling of mesoscale tropospheric humidity fluctuations, *Geophys. Res. Lett.*, *27*, 337–380, 2000.

Dessler, A. E., and H. Kim, Determination of the amount of water vapor entering the stratosphere based on Halogen Occultation Experiment (HALOE) data, *J. Geophys. Res.*, *104*, 30,605–30,607, 1999.

Ehret, G., K. P. Hoinka, J. Stein, A. Fix, C. Kiemle, and G. Poberaj, Low stratospheric water vapor measured by an airborne DIAL, *J. Geophys. Res.*, *104*, 31,351–31,359, 1999.

Gierens, K., and P. Spichtinger, On the size distribution of ice-supersaturated regions in the upper troposphere and lowermost stratosphere, *Ann. Geophys.*, *18*, 499–504, 2000.

Gierens, K., U. Schumann, M. Helten, H. Smit, and A. Marenco, A distribution law for relative humidity in the upper troposphere and lower stratosphere derived from three years of MOZAIC measurements, *Ann. Geophys.*, *17*, 1218–1226, 1999.

Gierens, K., U. Schumann, M. Helten, H. Smit, and P. H. Wang, Ice-supersaturated regions and subvisible cirrus in the northern midlatitude upper troposphere, *J. Geophys. Res.*, *105*, 22,743–22,753, 2000.

Grossman, K. U., D. Offerman, O. Gusev, J. Oberheide, M. Riese, and R. Spang, The CRISTA 2 Mission, *J. Geophys. Res.*, *107*, doi:10.1029/2001JD000667, in press, 2002.

Haynes, P., and E. Shuckburgh, Effective diffusivity as a diagnostic of atmospheric transport, 2, Troposphere and lower stratosphere, *J. Geophys. Res.*, *105*, 22,795–22,810, 2000.

Helten, M., H. G. J. Smit, W. Straeter, D. Kley, P. Nédélec, M. Zoeger, and R. Busen, Calibration and performance of automatic compact instrumentation for the measurement of relative humidity from passenger aircraft, *J. Geophys. Res.*, *103*, 25,643–25,652, 1998.

Helten, M., H. G. J. Smit, D. Kley, J. Ovarlez, H. Schlager, R. Baumann, U. Schumann, P. Nédélec, and A. Marenco, In-flight comparison of MOZAIC and POLINAT water vapor measurements, *J. Geophys. Res.*, *104*, 26,087–26,096, 1999.

Hintsa, E. J., E. M. Weinstock, J. G. Anderson, R. D. May, and D. F. Hurst, On the accuracy of in situ water vapor measurements in the troposphere and lower stratosphere with the Harvard Lyman-α hygrometer, *J. Geophys. Res.*, *104*, 8183–8189, 1999.

Holton, J. R., P. H. Haynes, M. E. McIntyre, A. R. Douglas, R. B. Rood, and L. Pfister, Stratosphere–troposphere exchange, *Rev. Geophys.*, *33*, 403–439, 1995.

Jensen, E. J., W. G. Read, J. Mergenthaler, B. J. Sandor, L. Pfister, and A. Tabazadeh, High humidities and subvisible cirrus near the tropical tropopause, *Geophys. Res. Lett.*, *26*, 2347–2350, 1999.

Keil, M., M. Heun, J. Austin, W. Lahoz, G. P. Lou, and A. O'Neill, The use of long-duration balloon data to determine the accuracy of stratospheric analyses and forecasts, *J. Geophys. Res.*, *106*, 10,299–10,312, 2001.

Kley, D., J. M. Russell III, and C. Phillips, SPARC assessment of upper tropospheric and stratospheric water vapour, *WCRP 113*, WMO/TD No. 1043, SPARC Rep. No. 2, 2000.

Mahlman, J. D., Dynamics of transport processes in the upper troposphere, *Science*, *276*, 1079–1083, 1997.

Marenco, A., et al., Measurement of ozone and water vapor by Airbus-in-service aircraft: The MOZAIC airborne program, An overview, *J. Geophys. Res.*, *103*, 25,631–25,642, 1998.

McCormack, J. P., R. Fu, and W. G. Read, The influence of convective outflow on water vapor mixing ratios in the tropical upper troposphere: An analysis based on UARS MLS measurements, *Geophys. Res. Lett.*, *27*, 525–528, 2000.

Nakamura, N., Two-dimensional mixing, edge formation, and permeability diagnosed in an area coordinate, *J. Atmos. Sci.*, *53*, 1524–1537, 1996.

Nedoluha, G. E., R. M. Bevilacqua, K. W. Hoppel, M. Daehler, E. P. Shettle, J. H. Hornstein, M. D. Fromm, J. D. Lumpe, and J. E. Rosenfeld, POAM III measurements of dehydration in the Antarctic lower stratosphere, *Geophys. Res. Lett.*, *27*, 1683–1686, 2000.

Offermann, D., K.-U. Grossmann, P. Barthol, P. Knieling, M. Riese, and R. Trant, Cryogenic Infrared Spectrometers and Telescopes for the Atmosphere (CRISTA) experiment and middle atmosphere variability, *J. Geophys. Res.*, *104*, 16,311–16,325, 1999.

Offermann, D., M. Jarisch, B. Schaeler, G. Eidmann, M. Langfermann, J. Oberheide, T. Wiemert, M. Riese, and C. Schiller, Trace gas densities and dynamics at and above the tropopause as derived from CRISTA data, *SPIE*, *4150*, 10–19, 2001.

Ovarlez, J., P. van Velthoven, and H. Schlager, Water vapor measurements from the troposphere to the lowermost stratosphere: Some signatures of troposphere to stratosphere exchanges, *J. Geophys. Res.*, *104*, 16,973–16,978, 1999.

Ovarlez, J., P. van Velthoven, G. Sachse, S. Vay, H. Schlager, and H. Ovarlez, Comparison of water vapor measurements from POLINAT 2 with ECMWF analyses in high-humidity conditions, *J. Geophys. Res.*, *105*, 3737–3744, 2000.

Pan, L., S. Solomon, W. Randel, J.-F. Lamarque, P. Hess, J. Gille, E-W. Chiou, and M. P. McCormick, Hemispheric asymmetries and seasonal variations of the lowermost stratosphere water vapor and ozone derived from SAGE II data, *J. Geophys. Res.*, *102*, 28,177–28,184, 1997.

Pan, L. L., E. J. Hintsa, E. M. Stone, E. W. Weinstock, and W. R. Randel, The seasonal cycle of water vapor and saturation vapor mixing ratio in the extratropical lowermost stratosphere, *J. Geophys. Res.*, *105*, 26,519–26,530, 2000.

Pfister, L., S. Scott, M. Loewenstein, S. Bowen, and M. Legg, Mesoscale disturbances in the tropical stratosphere excited by convection: Observations and effects on the stratospheric momentum budget, *J. Atmos. Sci.*, *50*, 1058–1075, 1993.

Read, W. G., et al., UARS MLS upper tropospheric humidity measurement: Method and validation, *J. Geophys. Res.*, *106*, 32,207–32,258, 2001.

Remsberg, E. E., P. B. Bhatt, and J. M. Russell III, Estimates of the water vapor budget of the stratosphere from UARS HALOE data, *J. Geophys. Res.*, *101*, 6749–6766, 1996.

Riese, M., R. Spang, P. Preusse, M. Ern, M. Jarisch, D. Offermann, and K. U. Grossmann, Cryogenic Infrared Spectrometers and Telescopes for the Atmosphere (CRISTA) data processing and atmospheric temperature and trace gas retrieval, *J. Geophys. Res.*, *104*, 16,349–16,367, 1999a.

Riese, M., X. Tie, G. Brasseur, and D. Offermann, Three-dimensional simulation of stratospheric trace gas distributions measured by CRISTA, *J. Geophys. Res.*, *104*, 16,419–16,435, 1999b.

Riese, M., V. Kuell, X. Tie, G. Brasseur, D. Offermann, G. Lehmacher, and A. Franzen, Modeling of nitrogen species measured by CRISTA, *Geophys. Res. Lett.*, *27*, 2221–2225, 2000.

Rose, K., and G. Brasseur, A three-dimensional model of chemically active trace species in the middle atmosphere during disturbed winter conditions, *J. Geophys. Res.*, *96*, 16,387–16,403, 1989.

Rosenfeld, D., and W. L. Woodley, Deep convective clouds with sustained supercooled liquid water down to −37.5°C, *Nature*, *405*, 440–442, 2000.

Schaeler, B., and M. Riese, Retrieval of water vapor in the tropopause region from CRISTA measurements, *Adv. Space Res.*, *27*(10), 1635–1640, 2001.

Smith, A. K., Numerical simulations of global variations of temperature, ozone, and trace species in the stratosphere, *J. Geophys. Res.*, *100*, 1253–1269, 1995.

Spang, R., M. Riese, G. Eidmann, D. Offermann, and P. H. Wang, A detection method for cirrus clouds using CRISTA 1 and 2 measurements, *Adv. Space Res.*, *27*(10), 1629–1634, 2001.

Spang, R., G. Eidmann, M. Riese, D. Offermann, P. Preusse, L. Pfister, and P. H. Wang, CRISTA observations of cirrus clouds around the tropopause, *J. Geophys. Res.*, *107*, doi:10.1029/2001JD000698, 2002.

Spivakovsky, C. M., et al., Three-dimensional climatological distribution of tropospheric OH: Update and evaluation, *J. Geophys. Res.*, *105*, 8931–8980, 2000.

Stone, E. M., L. Pan, J. Sandor, W. G. Read, and J. W. Waters, Spatial distributions of upper tropospheric water vapor measurements from the UARS microwave limb sounder, *J. Geophys. Res.*, *105*, 12,149–12,161, 2000.

Swinbank, R., and A. O'Neill, A stratosphere–troposphere data assimilation system, *Mon. Weather Rev.*, *122*, 686–702, 1994.

Teitelbaum, H., M. Moustaoui, C. Basdevant, and J. R. Holton, An alternative mechanism explaining the hygropause formation in tropical regions, *Geophys. Res. Lett.*, *27*, 221–224, 2000.

Udelhofen, P. M., and D. L. Hartmann, Influence of tropical cloud systems on the relative humidity in the upper troposphere, *J. Geophys. Res.*, *100*, 7423–7440, 1995.

Vay, S. A., B. E. Anderson, E. J. Jensen, G. W. Sachse, J. Ovarlez, G. L. Gregory, S. R. Nolf, J. R. Podolske, T. A. Slate, and C. E. Sorenson, Tropospheric water vapor measurements over the North Atlantic during the Subsonic Assessment Ozone and Nitrogen Oxide Experiment (SONEX), *J. Geophys. Res.*, *105*, 3745–3755, 2000.

Winker, D. M., and C. R. Trepte, Laminar cirrus observed near the tropical tropopause by LITE, *Geophys. Res. Lett.*, *25*, 3351–3354, 1998.

Zoeger, M., et al., Fast in situ stratospheric hygrometers: A new family of balloon-borne and airborne Lyman α photofragment fluorescence hygrometers, *J. Geophys. Res.*, *104*, 1807–1816, 1999.

G. Eidmann, Vacuumschmelze & CoKG, Hanau, Germany.

M. Jarisch, D. Offermann, M. Riese, and B. Schaeler, Department of Physics, University of Wuppertal, Wuppertal, Germany. (offerm@wpos2.physik.uni-wuppertal.de)

M. Langfermann, Daimler-Benz-Aerospace, Dornier GmbH, Friedrichshafen, Germany.

C. Schiller and H. G. J. Smit, Institute of Chemistry and Dynamics of the Geosphere, Research Center Juelich GmbH, Juelich, Germany.

W. G. Read, Jet Propulsion Laboratory, Pasadena, CA, USA.